Image Cover Sheet

CLASSIFICATION	SYSTEM NUMBER
UNCLASSIFIED	510363

TITLE

EFFECT OF UNDERMATCHING WELD METAL ON THE MEASURED FRACTURES TOUGHNESS OF HSLA 100 JOINTS

System Number:

Patron Number:

Requester:

Notes: Paper #20 contained in Parent Sysnum #510343

DSIS Use only:

Deliver to: DK

Effect of Undermatching Weld Metal on the Measured Fractures Toughness of HSLA 100 Joints

by

R. Yee[+], L. Malik[+] , and J. Morrison[++]

[+] Fleet Technology Limited, Kanata, Ontario

[++] Esquimalt Defence Research Detachment, Victoria, B.C.

ABSTRACT

Modern high strength steels such as HSLA 100 have excellent toughness and resistance to cold cracking in the heat affected zone, even when they are welded without pre-heat. Unfortunately, welding consumables with comparable strength, toughness, and resistance to cold cracking are not yet commercially available. As a result, fabricators are unable to fully exploit the cost advantages of welding such steels at this time. A potential solution to this problem is to weld the steels with undermatching consumables that have a lower tensile strength but higher intrinsic fracture toughness than the base metal. It is assumed that the higher intrinsic fracture toughness of the undermatching weld metal is sufficient to counter the higher crack driving force resulting from strain concentrations in the undermatching weld metal.

Although the effect of undermatching weld metal on measured fracture toughness has been inferred from numerical studies of the crack driving force in undermatching weld metal, there has been little experimental investigation of this effect. In the present study, HSLA steel plate was heat-treated to four lower yield strengths. Butt joints were subsequently made from these four steels as well as steel in the as-received condition. These joints were subsequently made from these four steels as well as steel in the as-received condition. These joints were fabricated with the same shielded metal arc welding procedure and consumable. Therefore, the weld metals in these joints were nominally identical with the same dilution, composition, microstructure, strength, and intrinsics toughness. Three-point bending specimens with standard deep notches and shallow notches were machined from each joint, and CTOD tests with these specimens were performed at various sub-zero temperatures. Traces of load versus load line displacement (LLD) and load versus crack mouth opening displacement (CMOD) were collected during these tests. This paper presents CTOD and J values calculated from both sets of traces, and examines the effect of undermatching weld metal on these values.

1.0 INTRODUCTION

Modern high strength steels such as HSLA 100 have excellent toughness and resistance to cold cracking in the heat affected zone, even when they are welded without pre-heat. Unfortunately, welding consumables with comparable strength, toughness, and resistance to cold-cracking are not yet commercially available. As a result, fabricators are unable to fully exploit the cost advantages of welding such steels at this time. A potential solution to this problem is to weld the steels with undermatching consumables that have a lower tensile strength but higher intrinsic fracture toughness than the base metal. It is assumed that the higher intrinsic fracture toughness of the undermatching weld metal is sufficient to counter the higher crack driving force resulting from strain concentrations in the weld metal. However, the magnitude of the required increase in fracture toughness cannot be reliably quantified at this time because of uncertainties in the calculation of crack driving force in the undermatching weld metal in real structures and standard fracture mechanics specimens.

The following sets of equations are commonly used to calculate the crack driving force (**CTOD** and **J**) in standard Single Edge Notch Bend (**SENB**) specimens for fracture toughness tests of steels:

Set 1 (BS 5672 [1] and BS 7448 [2])

$$CTOD_{standard} = \frac{K^2(1-\nu^2)}{2\sigma_{YS}E} + \frac{.4(W-a_o)\,CMOD_p}{.4(W-a_o) + .6a_o + z}$$

$$J_{standard} = \frac{K^2(1-\nu^2)}{E} + \frac{2A_{LLD}}{B(W-a_o)}$$

Set 2 (Wang and Gordon [3])

$$CTOD_{CMOD} = \frac{K^2(1-\nu^2)}{2\sigma_{YS}E} + \frac{\eta_{C\text{-}C}A_{CMOD}}{\sigma_{YS}B(W-a_o)}$$

$$J_{CMOD} = \frac{K^2(1-\nu^2)}{E} + \frac{\eta_{J\text{-}C}A_{CMOD}}{B(W-a_o)}$$

where

$$K = \left(\frac{4F_{c,\,u,\,or\,m}}{BW^{.5}}\right) \times \frac{3\left(\frac{a_o}{W}\right)^{.5}\left[1.99 - \frac{a_o}{W}\left(1 - \frac{a_o}{W}\right)\left(2.15 - \frac{3.93a_o}{W} + \frac{2.7a_o^{\,2}}{W^2}\right)\right]}{2\left(1 + \frac{2a_o}{W}\right)\left(1 - \frac{a_o}{W}\right)^{1.5}}$$

$$\eta_{J\text{-}C} = 3.5 - 1.4167\left(\frac{a_o}{W}\right)$$

$$\eta_{C\text{-}C} = 4.292 - 1.667\left(\frac{a_o}{W}\right) + .304\left(\frac{\sigma_{UTS}}{\sigma_{YS}}\right)^2 - 2.0\left(\frac{\sigma_{UTS}}{\sigma_{YS}}\right)$$

K is the elastic stress intensity factor, $\mathbf{a_o}$ is the depth of the fatigue pre-crack and its starter notch; F is the applied load; $\mathbf{CMOD_p}$ is the plastic component of the crack mouth opening displacement; A_{CMOD} is the area bounded by the applied force versus crack mouth opening displacement curve up to **F** and the elastic unloading line from **F**; A_{LLD} is the area bounded by the applied force versus load-line displacement curve up to **F** and the elastic unloading line from **F**; **W** is the width of the specimen; **z** is the distance from the mouth of the starter notch to the point of attachment between the extensometer and its knife edges; ν is the Poisson ratio of the material; **E** is the material's modulus of elasticity; σ_Y is the material's yield strength, and σ_{UTS} is the material's ultimate tensile strength.

Both sets of equations are empirical and have been calibrated against experimental data for homogeneous test specimens. The first set of equations is only intended for $\mathbf{a_o/W}$ ratios between .45 and .55, whereas the second set of equations is applicable to $\mathbf{a_o/W}$ ratios between .1 and .6. For the same base metal, specimen geometry, and applied load, the plastic strain distribution and the limit load of test specimens with either undermatching or overmatching weld metal differ from that in homogeneous test specimens, Therefore, in principle, the equations should not be applied to test specimens with mis-matched weld metal. However, recent elasto-plastic finite element analyses by Kirk and Dodd [4] have indicated that the strain concentration effect and limit load effect in **SENB** test specimens with mis-matched weld metal tend to offset each other and that the aforementioned equations are sufficiently accurate for test specimens with up to +/-20% mis-match between the yield strengths of the weld metal and base metal.

This paper presents fracture toughness data (**CTOD** and **J**) for shallow notch and deep notch **SENB** specimens that were machined from HSLA 100 steel butt joints with the same weld metal but base metal heat-treated to different tensile strengths. These measured fracture toughness values provide an indirect indication of the effect of weld mis-match on calculated driving force force since the specimens had the same weld metal and therefore the same intrinsic fracture toughness.

2.0 EXPERIMENTAL PROCEDURE

Standard crack tip opening displacement (**CTOD**) tests were conducted with 94 Single Edge Notch Bend (**SENB**) specimens. These specimens were machined from five series of butt joints (18 to 20 specimens from each series). Each series of butt joints were fabricated from the same weld metal but different base metals, viz., HSLA 100 steel heat treated to different yield strengths (FIgures 1 and 2). The latter strengths were chosen to achieve five levels of mis-match between the yield strength of the weld metal (YS_{weld}) and the yield strength of the base metal (YS_{base}): $(YS^{weld}-Y_{base})/YS_{base}$ = -.295, -.165, -.088, -.019, and +.156. The dimensions of these specimens and the orientation of the weld metal in these specimens are shown in Figure 3. A 12 mm deep notch was machined in the weld metal of half of the specimens from each series, while a 3 mm deep notch was machined in the weld metal of the remaining specimens from each series. These through-thickness notches were machined with a slitting wheel which produced the notch tip geometry shown in the inset of Figure 3.

A 2 to 3 mm deep fatigue crack was initiated at the notch tip of each specimen by cyclically loading the specimen in three-point bending. This pre-cracking was performed in a Pegasus servo-hydraulic test machine at an R-ratio of .1. Prior to this operation, the notch tip was plastically compressed in the through-thickness direction (1% plastic strain) with a 12.7 mm diameter platen. The maximum applied loads for the shallow notch specimens and deep notch specimens were initially maintained at 24.7 kN and 10.4 kN, respectively, until a .5 mm deep fatigue crack was visually detected at the edges of the starter notch. The maximum applied loads for the shallow notch specimens and deep notch specimens were then reduced to 19.1 kN and 7.9 kN, respectively, for the next .5 to 1.0 mm of fatigue crack growth[1]. The maximum applied loads for the shallow notch specimens and deep notch specimens were maintained at 13.6 kN and 5.4 kN, respectively, for the final 1.0 to 1.5 mm of fatigue crack $growth_1$. The latter loads produced a maximum stress intensity factor of 700 $MN/mm^{3/2}$ at the final crack tip.

The **CTOD** tests were conducted with the **SENB** specimens immersed in an alcohol bath. These tests were performed under displacement control in a Baldwin servo-hydraulic test machine with the three-point bending fixture. The load-line displacement rate (quasi-static) was approximately .5 mm per minute. The deep notch specimens were tested at -10°C, -30°C, -40°C, and -60°C, while the shallow notch specimens were tested at -40°C and -60°C (see Table 1 for test matrix). These temperatures were obtained by cooling the alcohol bath with dry ice to a temperature 3°C below the desired test temperature.

---

[1] visually measured at the edges of the starter notch

Table 1: Matrix of specimens for fracture toughness tests.

Deep notch specimens

$\frac{YS_{weld}-YS_{base}}{YS_{base}}$	-10°C	-30°C	-40°C	-60°C
-.295		3	3	3
-.165	3		3	3
-.088	3	1	3	3
-.019		4	3	3
+.156	1	2	3	3

Shallow notch specimens

$\frac{YS_{weld}-YS_{base}}{YS_{base}}$	-10°C	-30°C	-40°C	-60°C
-.295			5	4
-.165			5	4
-.088			5	5
-.019			5	5
+.156			5	4

Three quantities were monitored during each test: applied force (**F**), crack mouth opening displacement (**CMOD**), and load-line displacement (**LLD**). Load-line displacement, which was defined as the vertical displacement of the notch mouth relative to a comparator bar, was measured with a proximity probe. Crack mouth opening displacement was measured with an extensometer that was attached to knife edges at the mouth of the starter notch. Applied force was measured with a load cell in series with the loading ram and hydraulic actuator. Data from these transducers was collected with a 16 bit data acquisition system at a sampling rate of 3 Hz. Each test was terminated when the applied force reached a maximum plateau or abruptly decreased by more than 5%. In every case, a plateau or peak in the applied force was reached before a pop-in occurred, where a pop-in was defined as a less than 5% drop in the applied force followed by an increase in the applied force to a level at least as high as the applied force at the start of the load drop.

Once the **CTOD** tests were completed, the specimens were soaked in liquid nitrogen and broken apart by rapidly loading them in the Baldwin's three-point bending fixture. The final fracture surfaces of the specimens were then examined under a stereomicroscope. These examinations identified three basic modes of failure during the **CTOD** tests:

1. arrested unstable cleavage,

2. stable ductile tearing followed by arrested unstable cleavage, and

3. stable ductile tearing.

These three modes are herein referred to as **Mode c**, **Mode u**, and **Mode m** failures, respectively.

As stated earlier, each test was terminated when the applied force reached a maximum plateau or peaked and then abruptly decreased by more than 5%. In every case, a plateau or peak in the applied force was reached before a pop-in had occurred, a pop-in being defined as a less than 5% drop in the applied force followed by an increase in the applied force to a level at least as high as the applied force at the start of the load drop. The peak forces coincided with the onset of unstable cleavage in **Mode c** and **Mode u** failures, whereas the force plateaus were reached in **Mode m** failures. The force peak in a **Mode c** or **Mode u** failures is herein referred to as $\mathbf{F_c}$ or $\mathbf{F_u}$, respectively, while the maximum force in a **Mode m** failure is herein referred to as $\mathbf{F_m}$.

Equations 1 and 3 were used to independently calculate the **CTOD** value at $\mathbf{F_c}$, $\mathbf{F_u}$, or $\mathbf{F_m}$ for each specimen, while Equations 2 and 4 were used to independently calculate the **J** value at $\mathbf{F_c}$, $\mathbf{F_u}$, or $\mathbf{F_m}$ for each specimen. As indicated earlier, Equations 1 and 2 are only intended for $\mathbf{a_o/W}$ ratios between .45 and .55. Nevertheless, these equations were applied to the shallow notch specimens as well as the deep notch specimens. For the purposes of this project, all calculations were based on material properties at room temperature. The average crack depth of the fatigue pre-crack and its starter notch was based on nine equally-spaced measurements across the crack front with a travelling microscope. A Simpson's rule algorithm (1% convergence tolerance) was used to numerically evaluate the areas under the applied load versus crack mouth opening displacement curves and applied load versus load-line displacement curves, while the areas under the elastic unloading lines were calculated analytically. The slopes of the elastic unloading lines were derived from empirical solutions for the elastic compliances of the **SENB** specimens in their initial configuration.

Fracture toughness values could not be derived for Specimens AR-2, 2-7, 6-2, 6-7, and 72-1 because the raw data for these specimens was not properly stored by the data acquisition system. In addition, $J_{standard}$ values could not be derived for Specimens AR-1, 1-1, 1-4, 2-1, 2-2, 6-1, and 6-3 because the proximity probe for measuring load-line displacement was improperly mounted.

3.0 RESULTS

The measured fracture toughness values for the shallow notch specimens are plotted against temperature in Figures 4-7, while the measured fracture toughness values for the deep notch specimens are plotted against temperature in Figures 8-11. The failure mode of each specimen is identified in these figures.The following observations were made from the aforementioned figures:

1. The fracture toughness values for the shallow notch specimens tended to increase with increasing temperature. The majority of these specimens failed by **Mode u**. Of the remaining specimens, only one failed by **Mode m** and only three failed by **Mode c**. This indicates that the two test temperatures for the shallow notch specimens (-40°C and -60°C) were well within the ductile-brittle transition for these specimens.

2. The measured fracture toughness values for the deep notch specimens tested tested at -30°C, -40°C, and -60°C tended to increase with increasing temperature, while the measured fracture toughness values for the deep notch specimens tested at -10°C were similar to the measured fracture toughness values for the deep notch specimens tested at -30°C. All of the deep notch specimens that were tested at -10°C failed by **Mode m**, whereas the deep notch specimens that were tested at -30°C failed by either **Mode u** or **Mode m**. Furthermore, most of the deep notch specimens that were tested at -60°C failed by **Mode c**; the remainder of these specimens failed by **Mode c**. This indicates that the start of the *upper shelf* for the fracture toughness of the deep notch specimens was somewhere between -10°C and -30°C while the lower part of the ductile-brittle transition region for these specimens was located near -60°C.

3. For a given temperature, the fracture toughness values for the shallow notch specimens were generally higher than the fracture toughness values for the deep notch specimens. This geometry dependence is related to the lower constraint in the shallow notch specimens, which promoted crack initiation by ductile tearing tearing rather than brittle cleavage.

4. The fracture toughness values for the shallow notch specimens were much more variable than the fracture toughness values for the deep notch specimens. In addition, the fracture toughness values in the upper ductile-brittle transition region of the deep notch specimens appeared to be more variable than the *upper shelf* fracture toughness values for these specimens. These differences can be attributed to two factors. First, the dominant mode of failure in these specimens was ductile crack initiation followed by brittle cleavage (i.e., **Mode u**). The measured fracture toughness values were associated with the onset of brittle cleavage. Second, cleavage in a **Mode u** failure occurs when the stress field ahead of the initial growing crack samples a critical particle. Therefore, the onset of cleavage is influenced by statistical sampling effects.

4.0 DISCUSSION

The mean, maximum, and minimum fracture toughness values for different notch depths and test temperatures are plotted against mismatch in Figures 12 to 16. None of these figures show an obvious relationship between measured fracture toughness and degree of weld mis-match, and statistical analyses of variance (ANOVA) failed to isolate any such relationship from the experimental scatter. This implies that the crack driving forces predicted by the equations were essentially independent of weld metal mis-match over the range of mis-match considered in this test program (-29.5% to +15.6%[2]), since all the test specimens had the same weld metal and therefore the same intrinsic fracture toughness. This is consistent with Kirk and Dodd's finite element analyses which show that the crack driving forces predicted by Equations 1-4 are essentially independent of the degree of weld metal mis-match in **SENB** specimens with up to +/- 20% weld metal mis-match.

According to Kirk and Dodd's finite element analyses, the equations based on the area underneath the applied load versus displacement (load-line or crack mouth opening) curve (i.e, Equations 3 and 4) are the most accurate for predicting the cracking driving force in **SENB** specimens with up to +/- 20% weld mis-match. However, Figures 17 to 20 indicate that Equation 1 is sufficiently accurate for predicting **CTOD** values greater than .1 mm and .2 mm in shallow notch specimens and deep notch specimens, respectively, while Equation 3 is sufficiently accurate for predicting J values with no lower bound. Figures 17 and 18 are plots of $(\mathbf{CTOD}_{standard}\text{-}\mathbf{CTOD}_{CMOD})/\mathbf{CTOD}_{CMOD}$ versus $\mathbf{CTOD}_{CMOD}$ for the shallow notch specimens and deep notch specimens, respectively. Figures 19 and 20 are plots of $(\mathbf{J}_{standard}\text{-}\mathbf{J}_{CMOD})/\mathbf{J}_{CMOD}$ versus $\mathbf{J}_{CMOD}$ for the shallow notch specimens and deep notch specimens, respectively. Figure 18 shows that the $\mathbf{CTOD}_{standard}$ values for the deep notch specimens were 4% to 6% lower than their corresponding $\mathbf{CTOD}_{CMOD}$ values when $\mathbf{CTOD}_{CMOD}$ exceeded ≈.3 mm, while Figure 17 shows that the $\mathbf{CTOD}_{standard}$ values for the shallow notch specimens were about 6% to 8% lower than their corresponding $\mathbf{CTOD}_{CMOD}$ values when $\mathbf{CTOD}_{CMOD}$ exceeded ≈.6 mm. Below these critical $\mathbf{CTOD}_{CMOD}$ values, the $\mathbf{CTOD}_{standard}$ values for both types of specimens exceeded their corresponding $\mathbf{CTOD}_{CMOD}$ values with the differences increasing exponentially with decreasing $\mathbf{CTOD}_{CMOD}$. In contrast, no exponential relationship was found between the $\mathbf{J}_{standard}$ and $\mathbf{J}_{CMOD}$ values for either the shallow notch specimens or the deep notch specimens. Figure 19 shows that the majority of $\mathbf{J}_{standard}$ values for the shallow notch specimens were within +/- 20% of their corresponding $\mathbf{J}_{CMOD}$ values, while Figure 20 shows that the majority of $\mathbf{J}_{standard}$ values for the deep notch specimens were 2% to 10% less than their corresponding $\mathbf{J}_{CMOD}$ values.

---

[2] $(YS_{weld}\text{-}YS_{base})/YS_{base}$

5.0 SUMMARY

HSLA 100 steel plate was heat-treated to four lower yield strengths, and butt joints were subsequently made from these four steels as well as steel in the as-received condition. These joints were fabricated with the same shielded metal arc welding procedure and consumable. Therefore, the weld metals in these joints were nominally identical with the same dilution, composition, microstructure, strength, and intrinsic toughness. 94 SENB specimens with deep and shallow notches were machined from the joints, and CTOD tests were performed at various sub-zero temperatures. Two sets of equations were used to calculate crack driving force: (1) the standard equations for deep notch SENB specimens and (2) recommended equations for shallow notch SENB specimens. There was no obvious effect of weld metal mis-match on the measured fracture toughness values. This implies that the crack driving forces predicted by the equations were essentially independent of weld metal mis-match over the range of mis-match considered in this test program (-29.5% to +15.6% with respect to yield strength), since all the test specimens had the same weld metal and therefore the same intrinsic fracture toughness.

6.0 REFERENCES

[1] BS 5762:1979,"Methods for Crack Opening Displacement (COD) Testing".

[2] BS 7448: Part 1: 1991,"Fracture Mechanics Toughness Tests. Method for the Determination of K_{IC}, Critical CTOD and Critical J Values of Metallic Materials."

[3] Wang, Y.Y. and Gordon, J.R., "The Limits of Applicability of J and CTOD Estimation Procedures for Shallow-Cracked SENB Specimens", Proc. of Conf. on Shallow Crack Fracture Mechanics, Toughness Tests, and Applications, Sept 23-24, 1992, The Welding Institute, Paper 28.

[4] Kirk, M.T. and Dodds, R.H.,"Effect of Weld Strength Mismatch on Elastic-Plastic Fracture Parameters", University of Illinois, Civil Engineering Studies, Structural Research Series No. 570, Report UILU-ENG-92-2008, Aug., 1992.

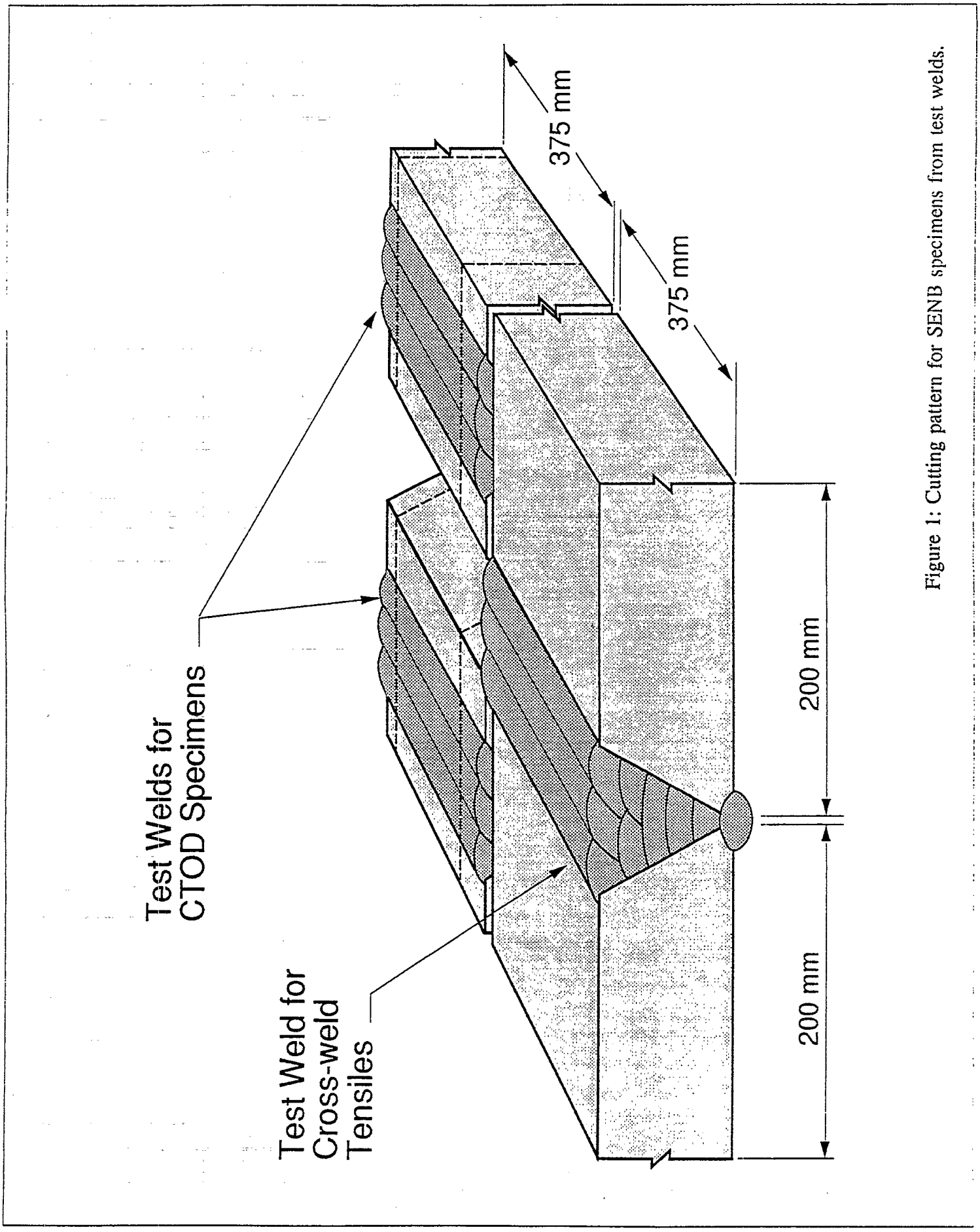

Figure 1: Cutting pattern for SENB specimens from test welds.

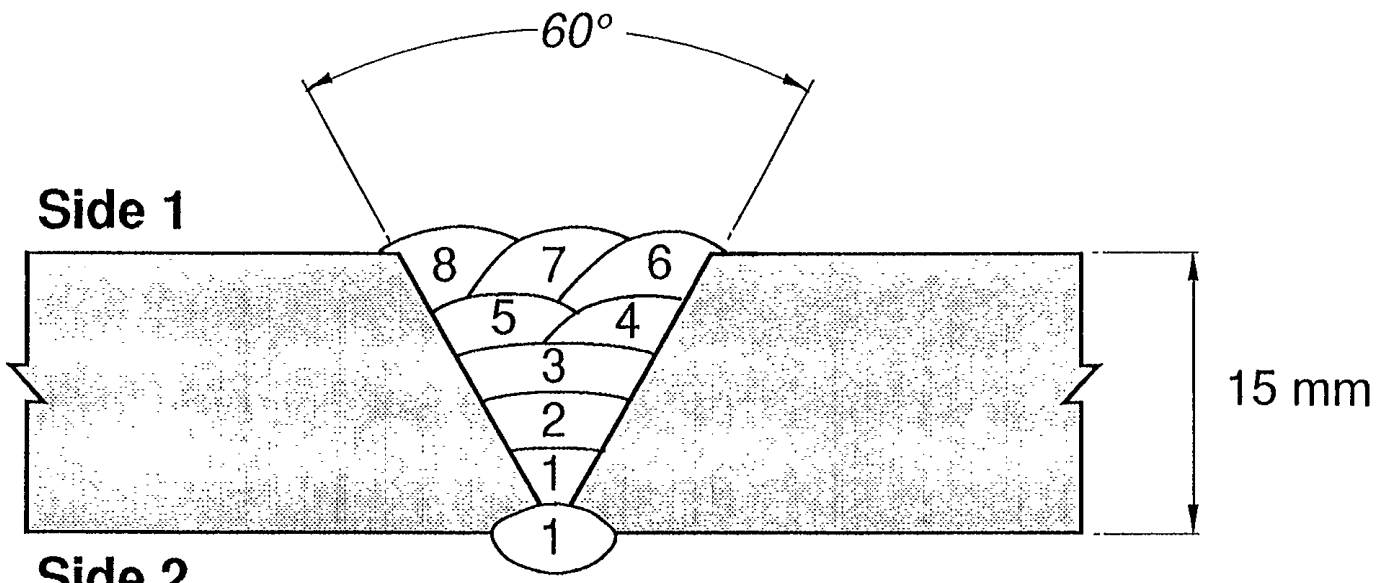

Material Specification:	HSLA 100
Welding Process:	Manual SMAW
Position of Welding:	1G
Filler Metal:	E10018M-1 Alloy Rods, 4 mm Dia.
Single or Multipass:	Multipass
Single or Multiple Arc:	Single (170 Amps, 22 Volts)
Preheat Temperature:	66° C
Interpass Temperature:	100° C
Preheat Method:	Propane Torch
Travel Speed:	130 - 200 mm/min.

Figure 2: Welding procedure for test welds.

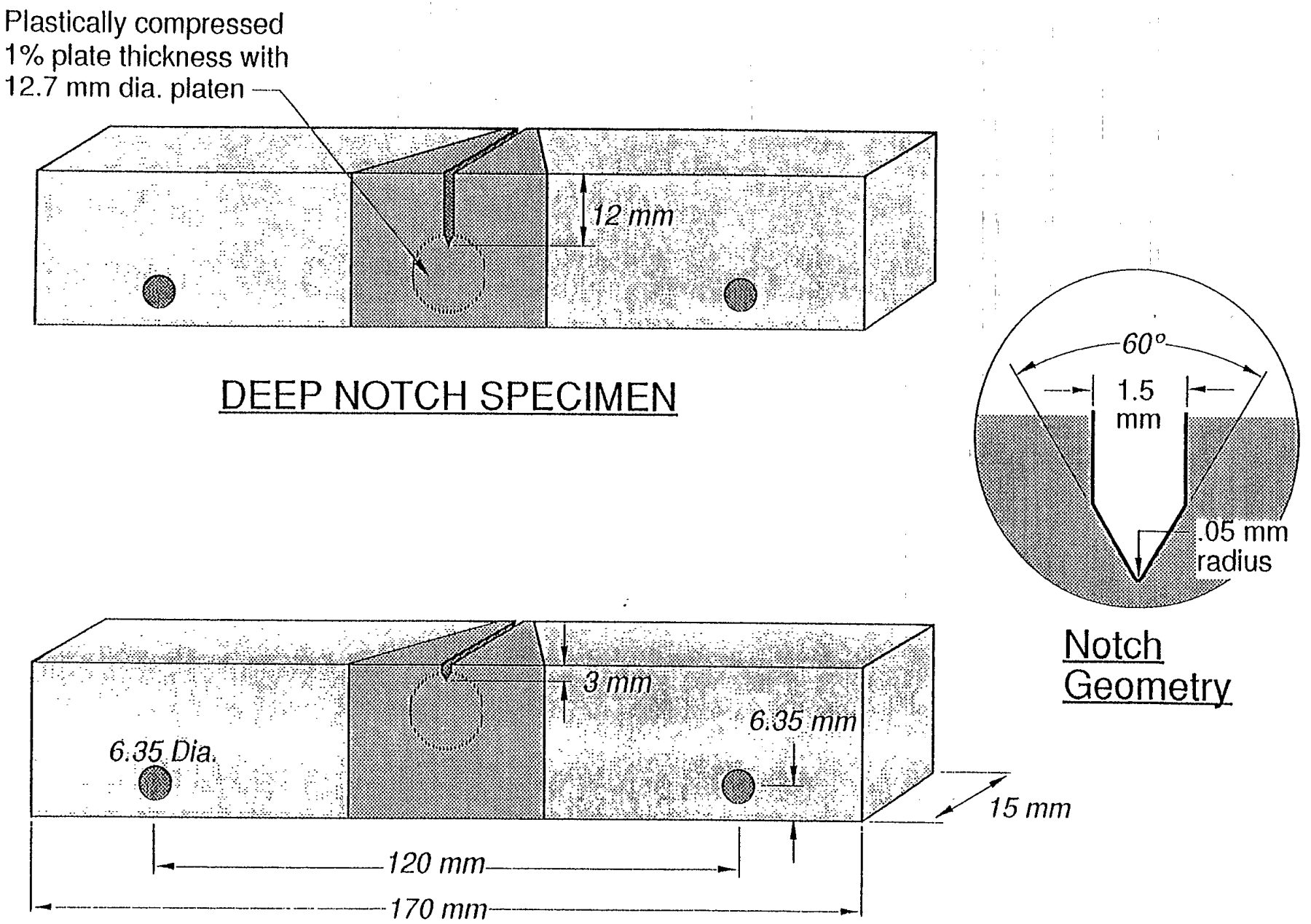

Figure 3 : SENB specimens for CTOD tests.

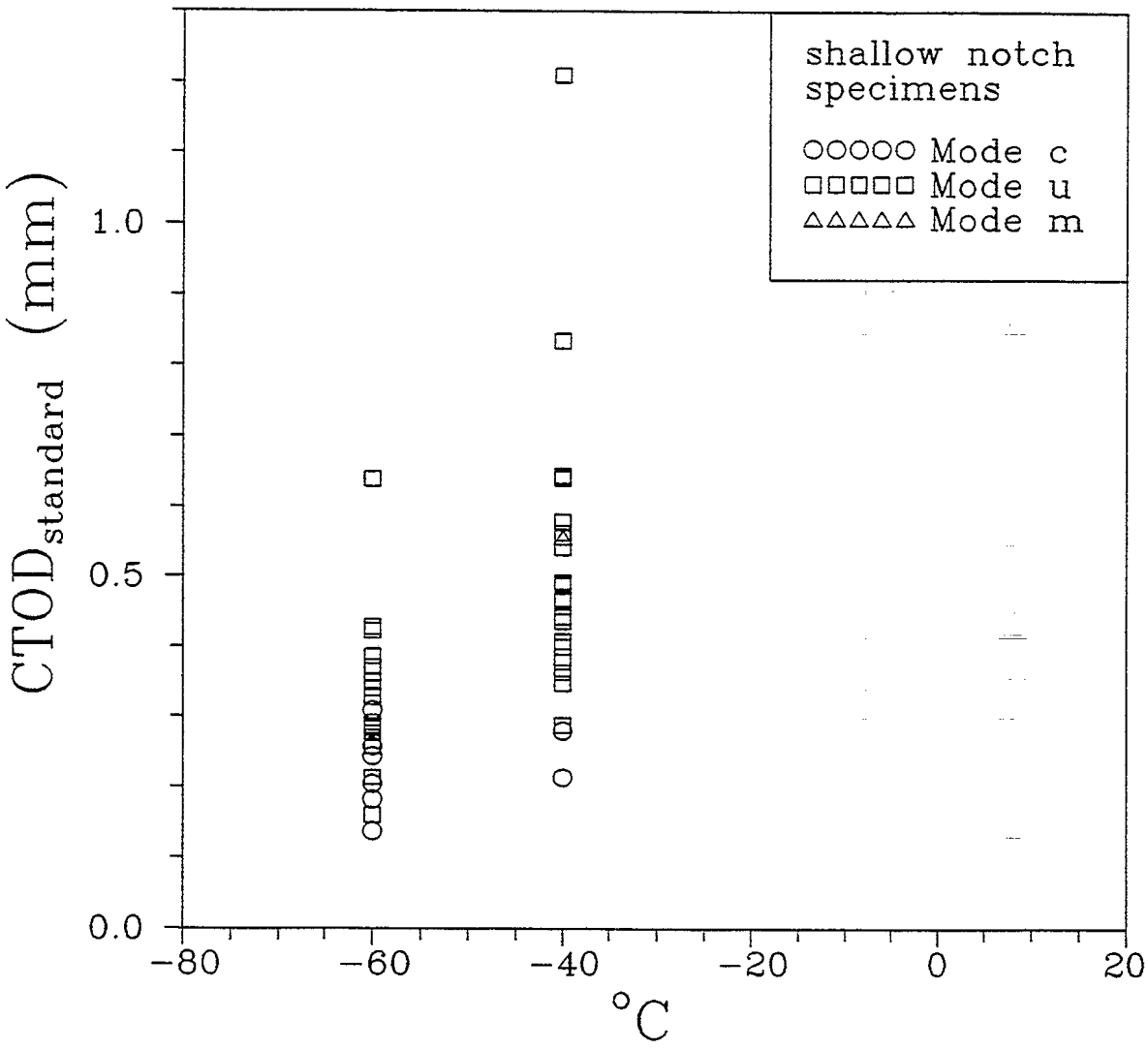

Figure 4: $CTOD_{standard}$ versus test temperature for shallow notch specimens.

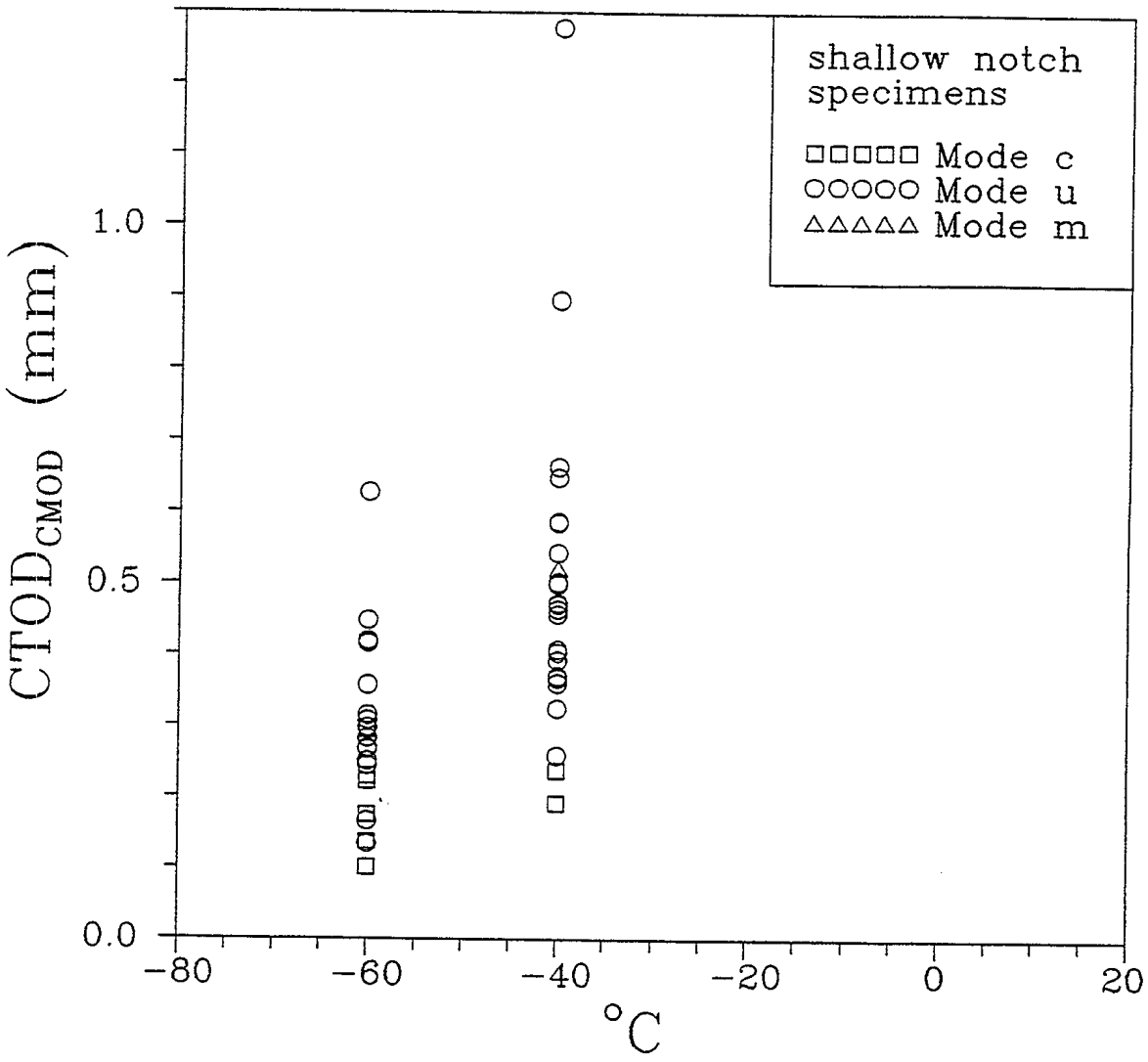

Figure 5: $CTOD_{CMOD}$ versus test temperature for shallow notch specimens.

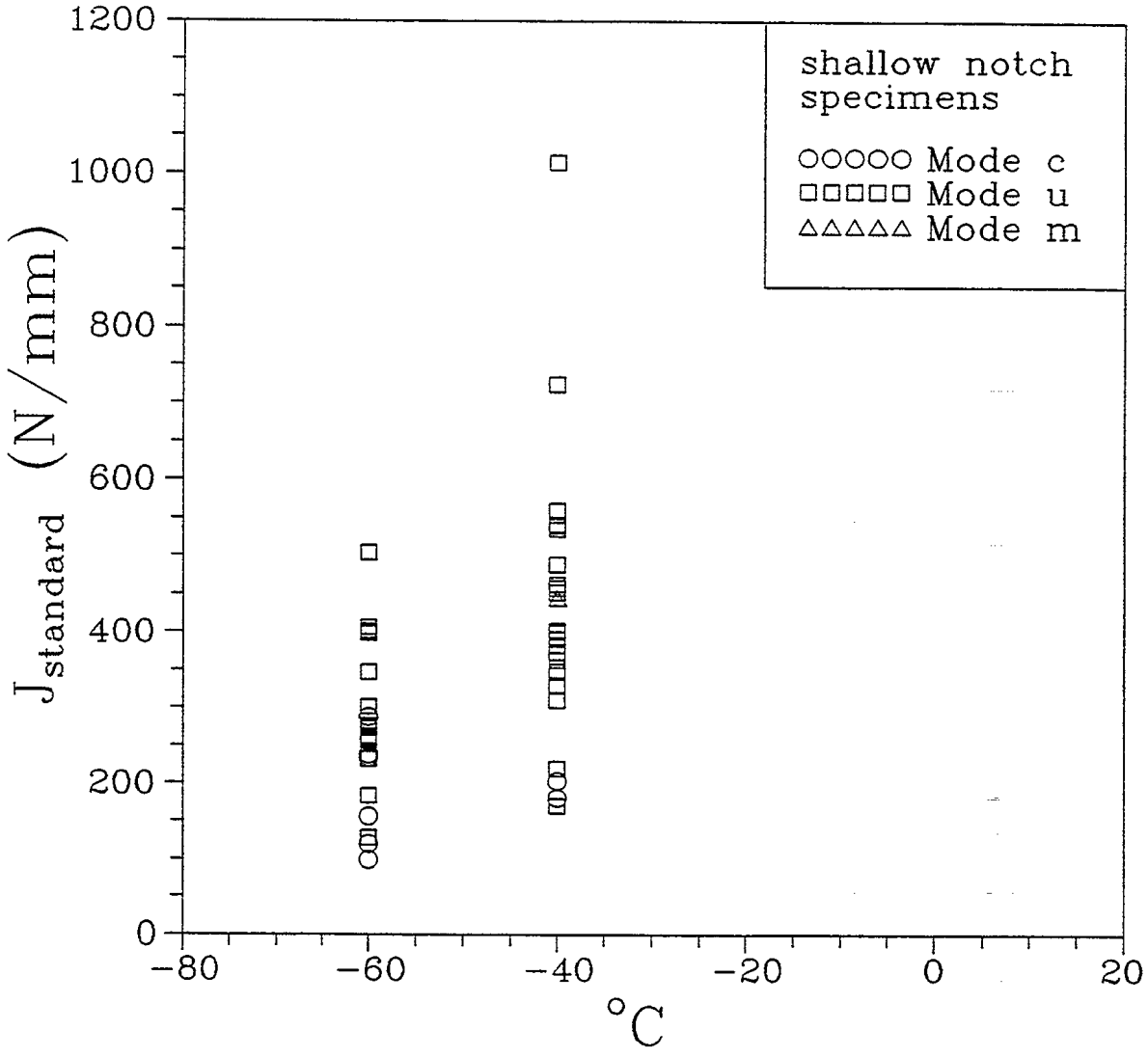

Figure 6 : $J_{standard}$ versus test temperature for shallow notch specimens.

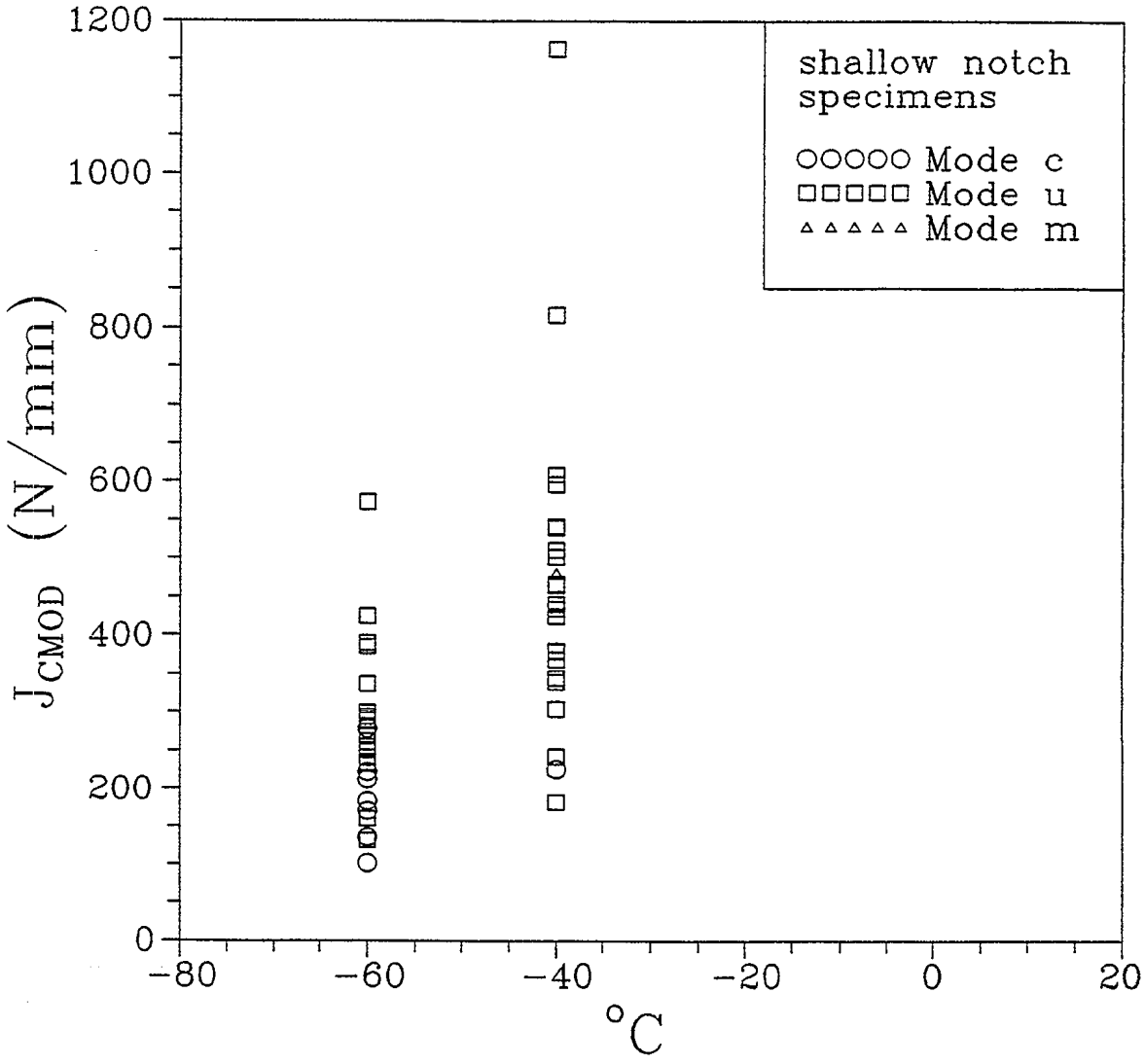

Figure 7: J_{CMOD} versus test temperature for shallow notch specimens.

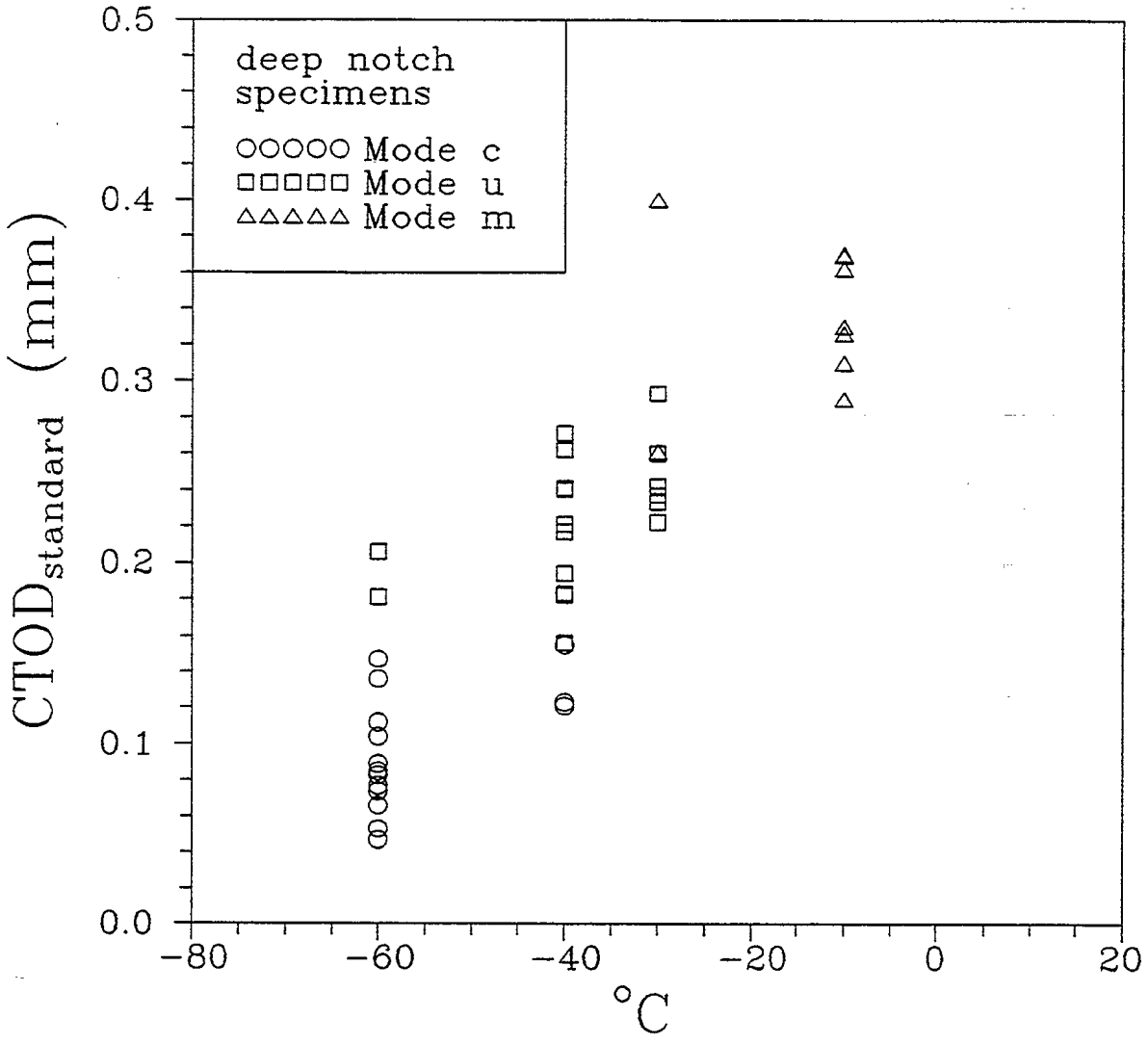

Figure 8 : $CTOD_{standard}$ versus test temperature for deep notch specimens.

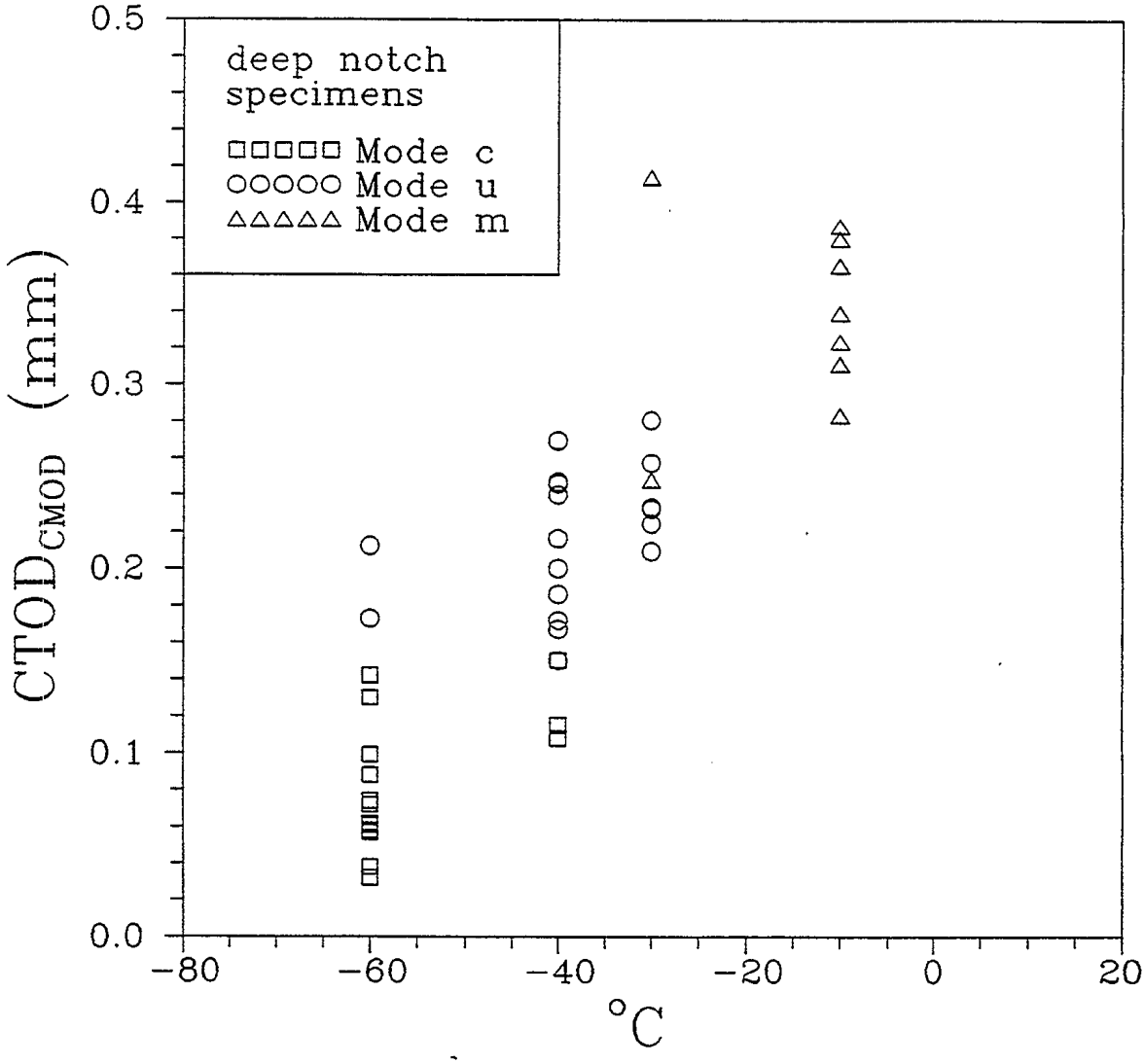

Figure 9 : $CTOD_{CMOD}$ versus test temperature for deep notch specimens.

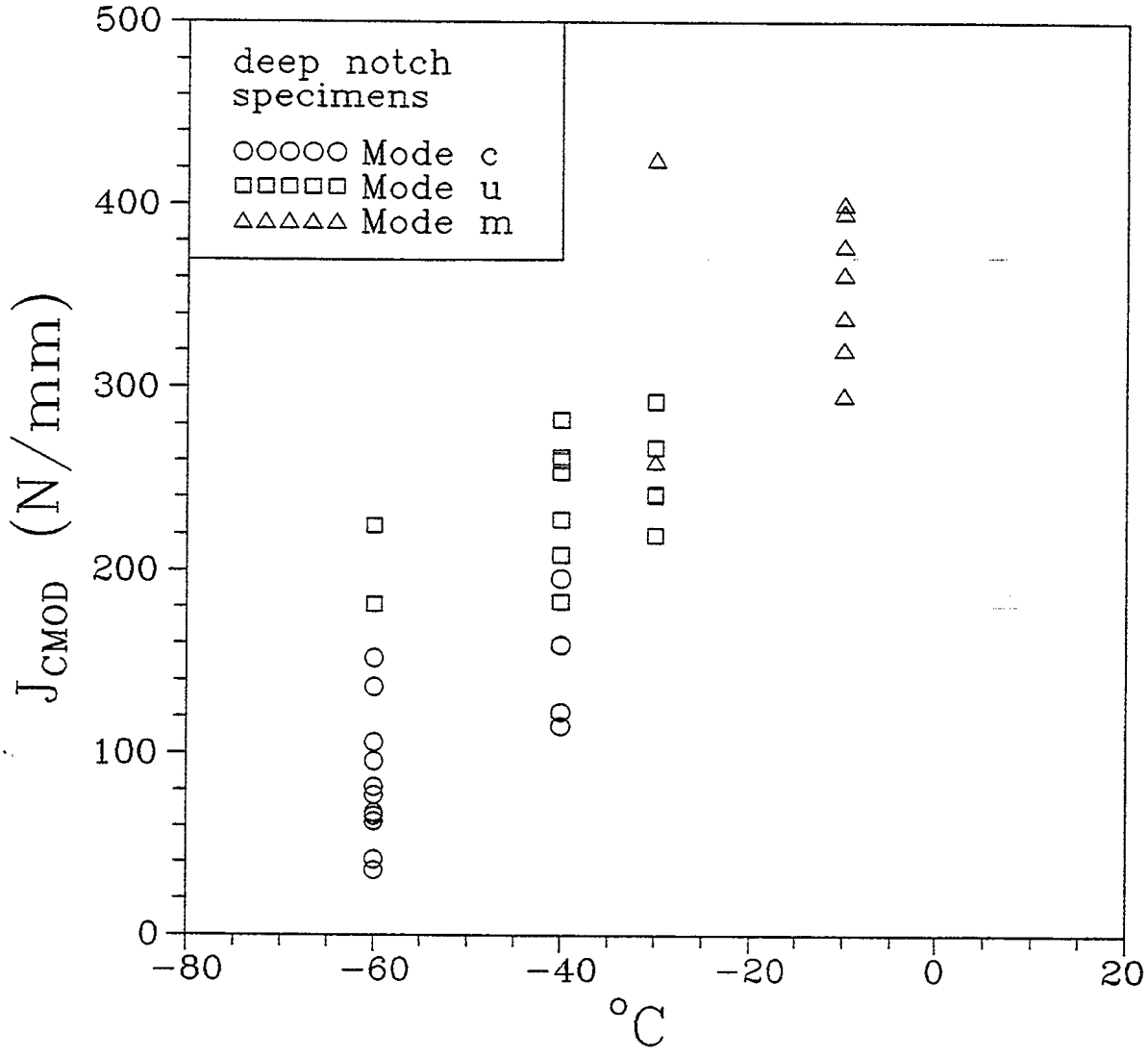

Figure 10: J_{CMOD} versus test temperature for deep notch specimens.

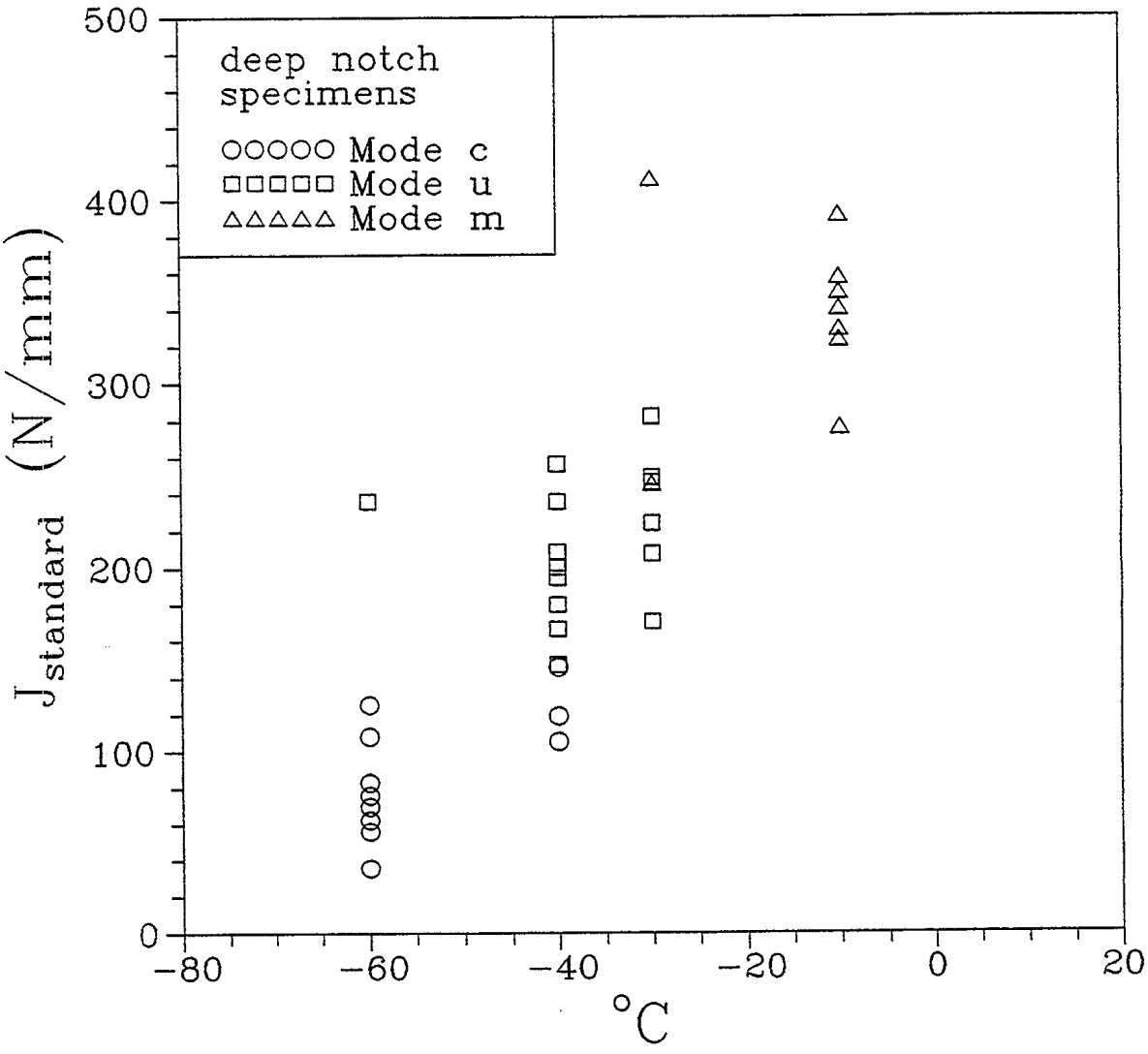

Figure 11: $J_{standard}$ versus test temperature for deep notch specimens.

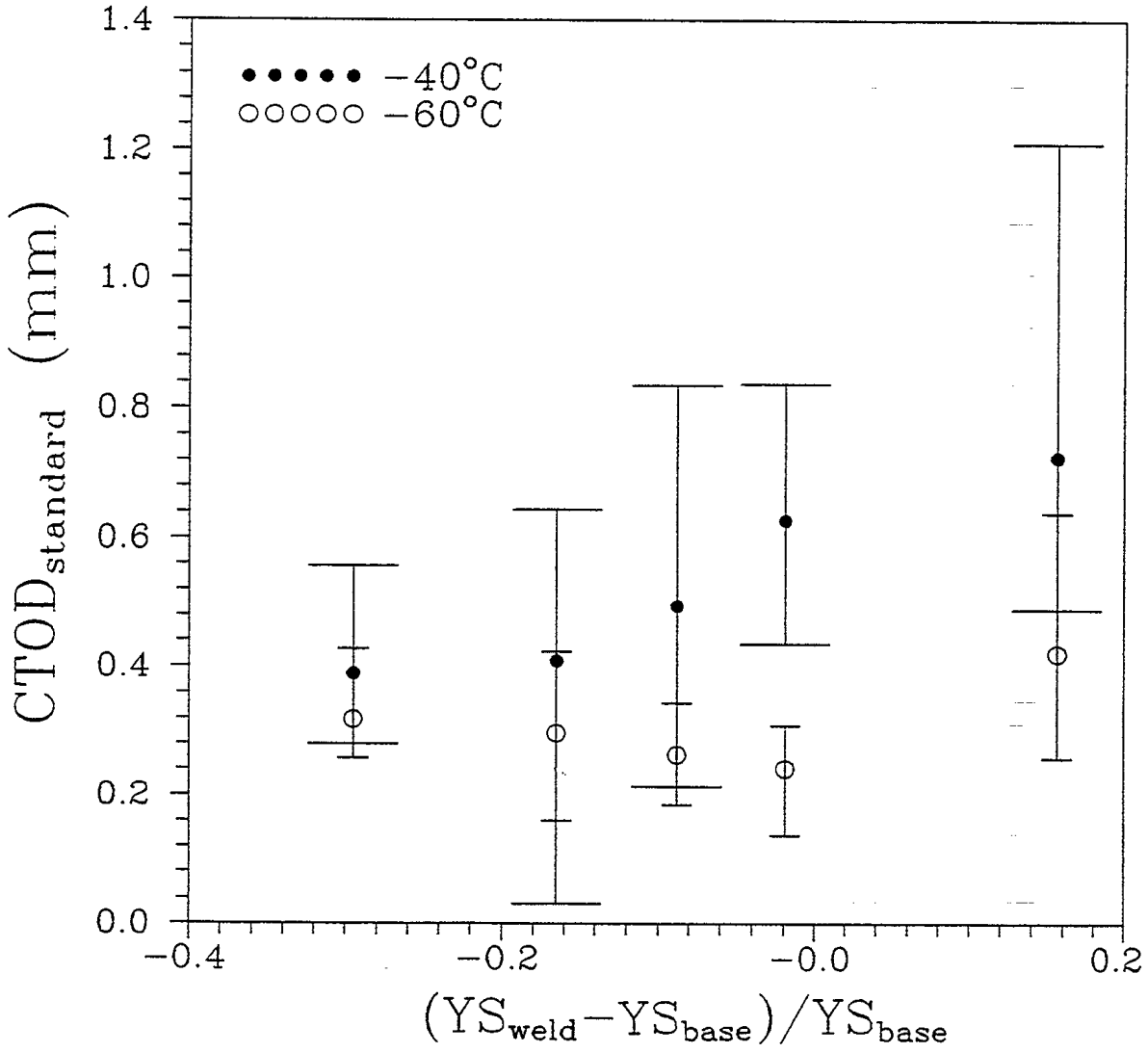

Figure 12: $CTOD_{standard}$ versus $(YS_{weld}-YS_{base})/YS_{base}$ for shallow notch specimens tested at -40°C and -60°C.

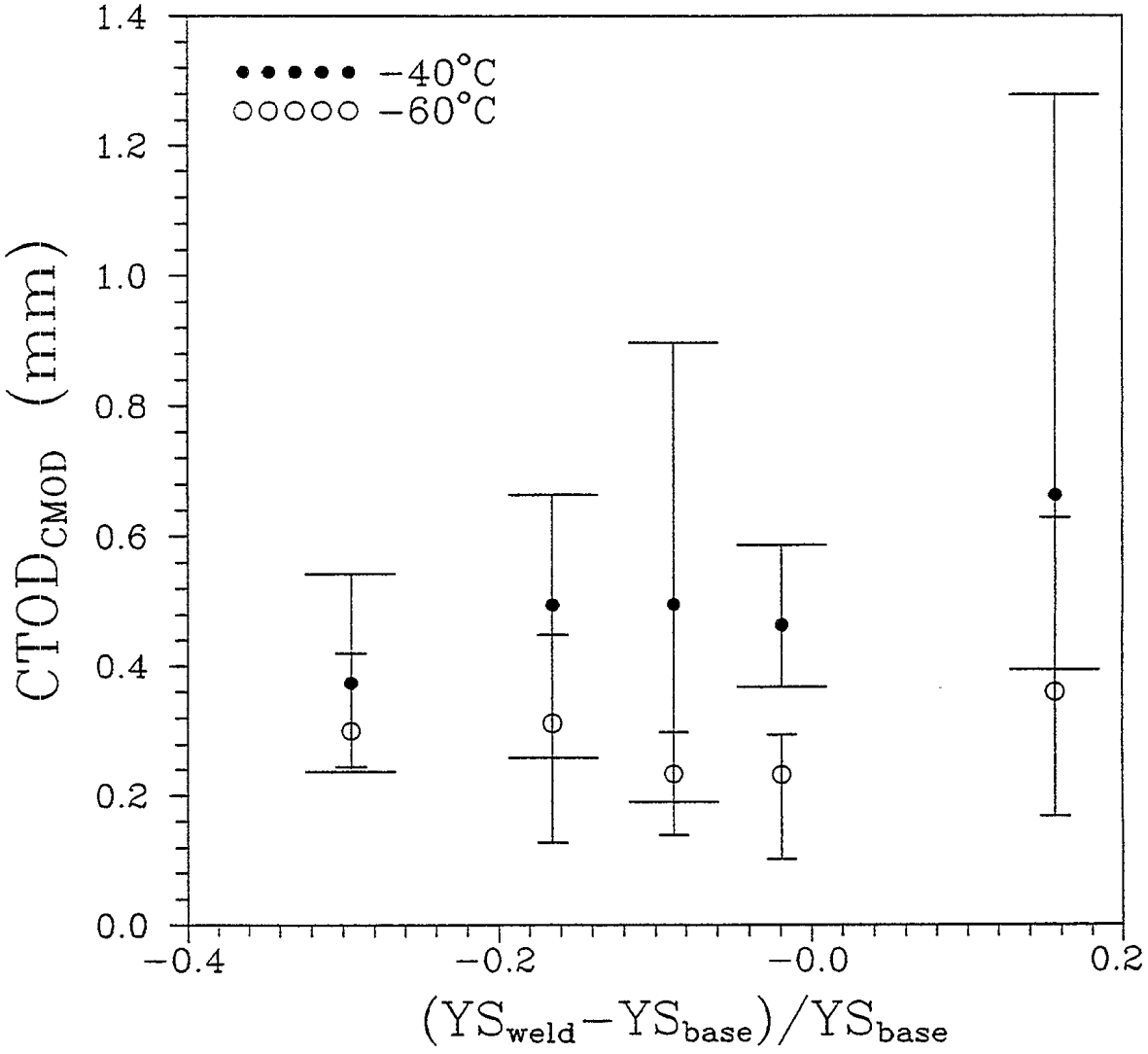

Figure 13: $CTOD_{CMOD}$ versus $(YS_{weld}-YS_{base})/YS_{base}$ for shallow notch specimens tested at -40°C and -60°C.

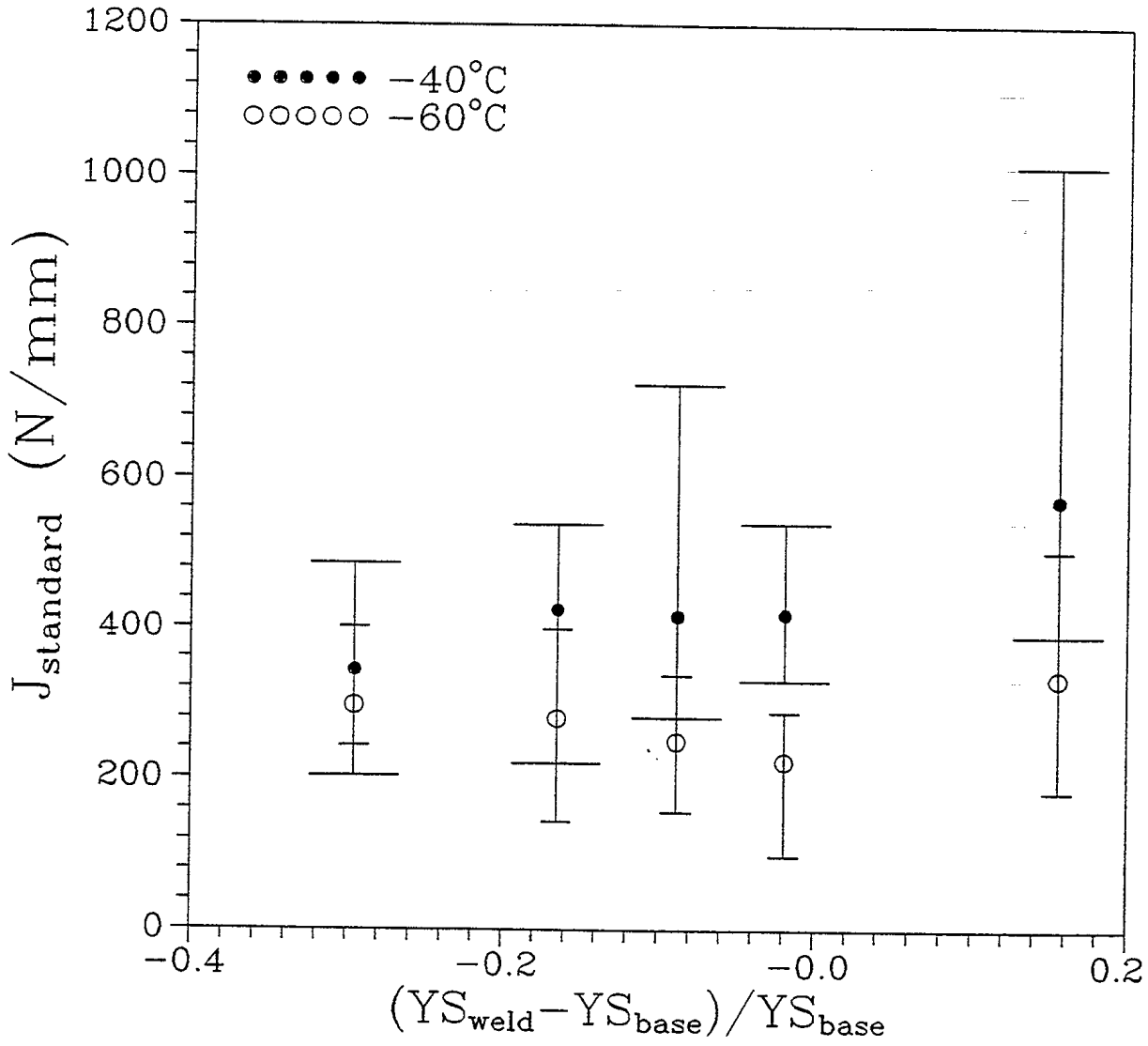

Figure 14: $J_{standard}$ versus $(YS_{weld}-YS_{base})/YS_{base}$ for shallow notch specimens tested at -40°C and -60°C.

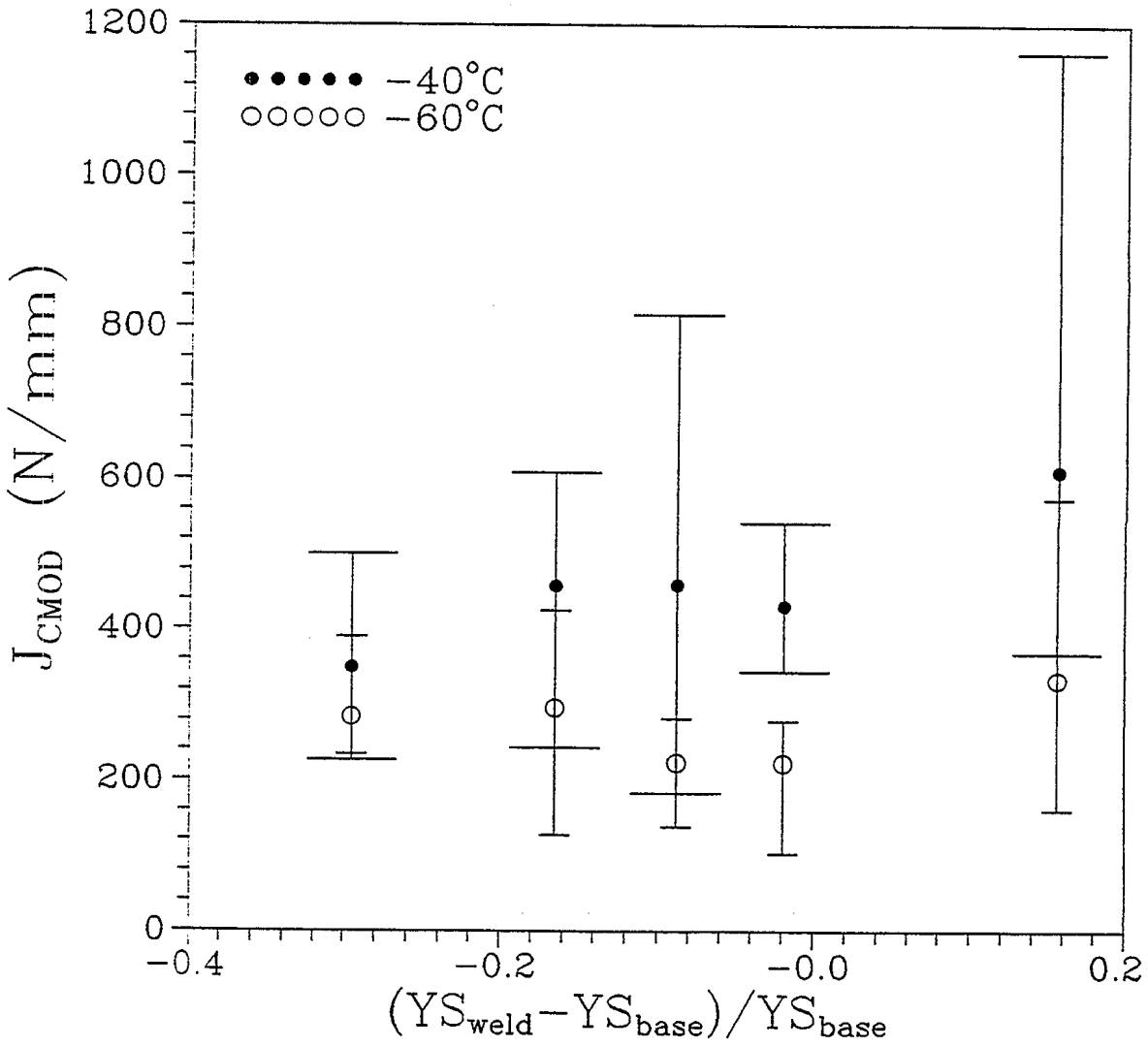

Figure 15: J_{CMOD} versus $(YS_{weld}-YS_{base})/YS_{base}$ for shallow notch specimens tested at -40°C and -60°C.

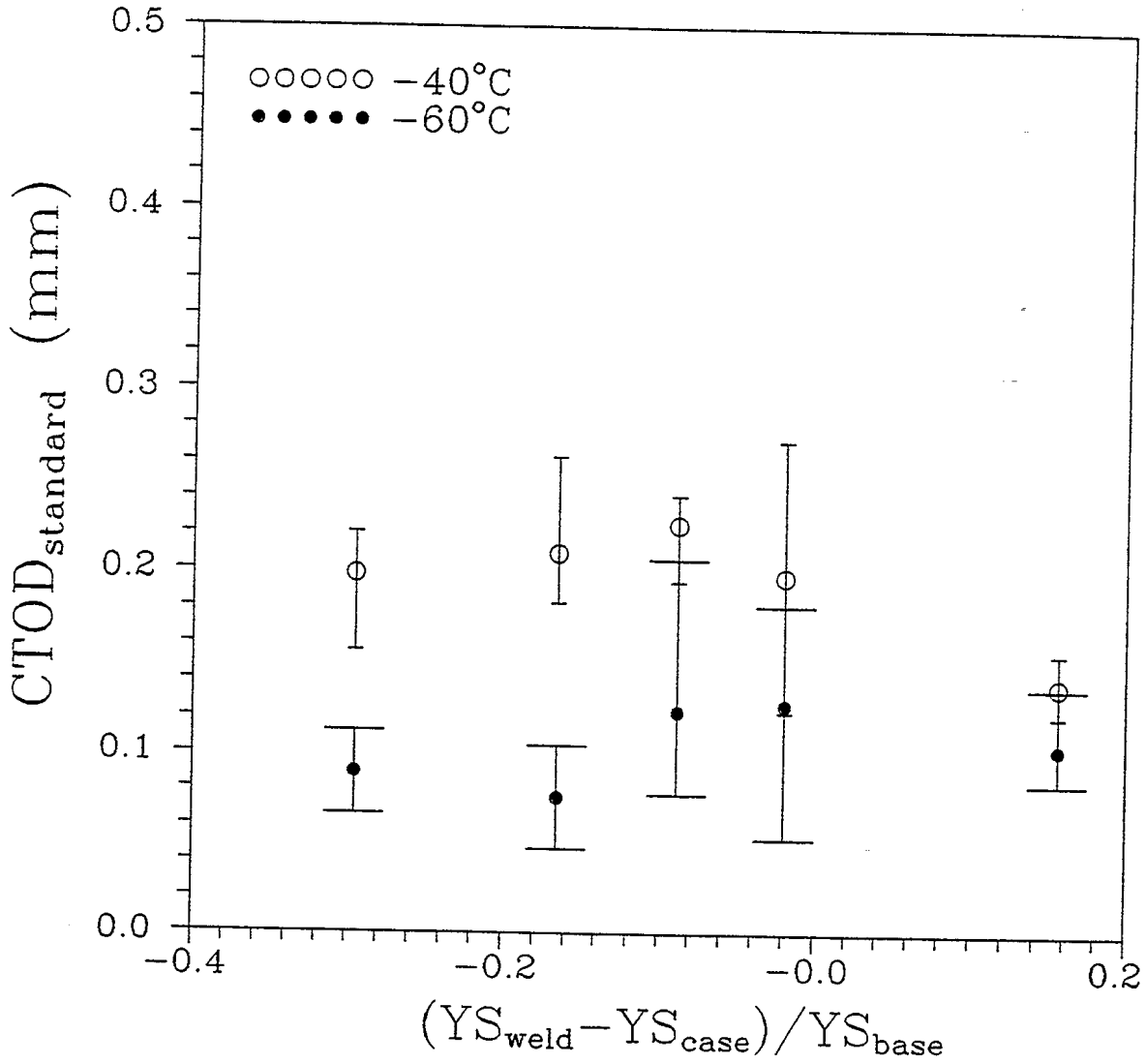

Figure 16: $CTOD_{standard}$ versus $(YS_{weld}-YS_{base})/YS_{base}$ for deep notch specimens tested at -40°C and -60°C.

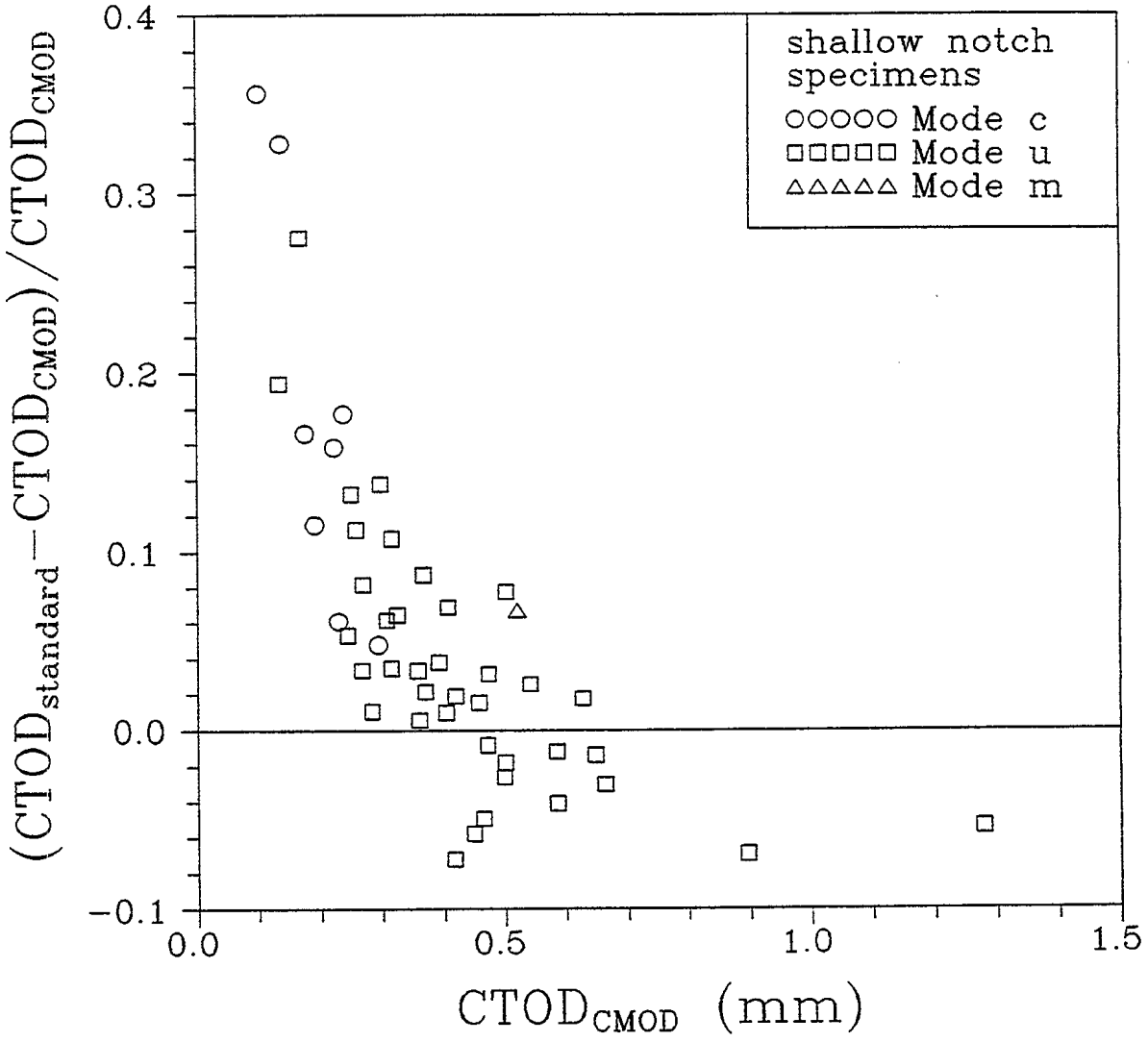

Figure 17: $(CTOD_{standard}-CTOD_{CMOD})/CTOD_{CMOD}$ versus $CTOD_{CMOD}$ for shallow notch specimens.

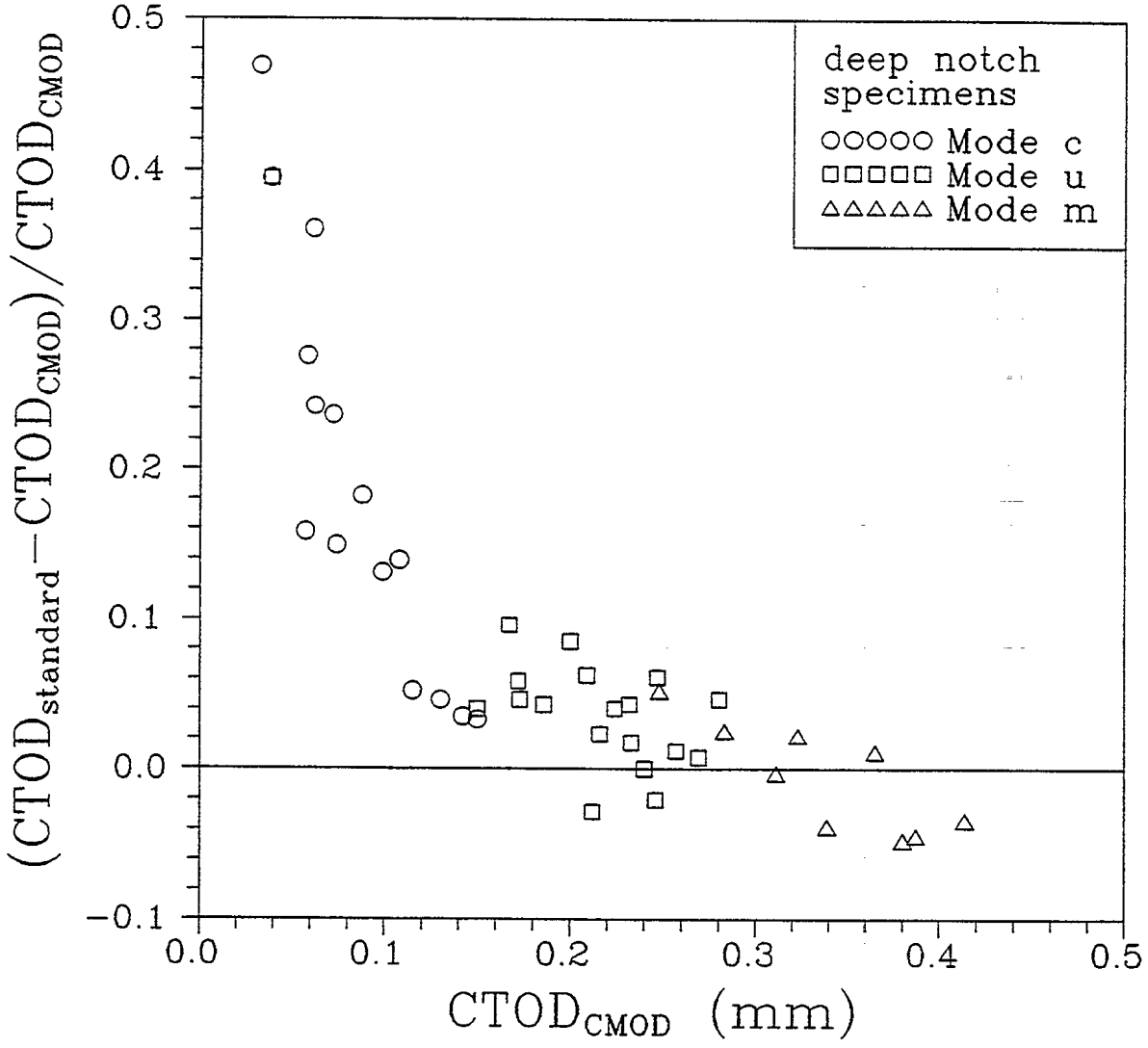

Figure 18: $(CTOD_{standard}-CTOD_{CMOD})/CTOD_{CMOD}$ versus $CTOD_{CMOD}$ for deep notch specimens.

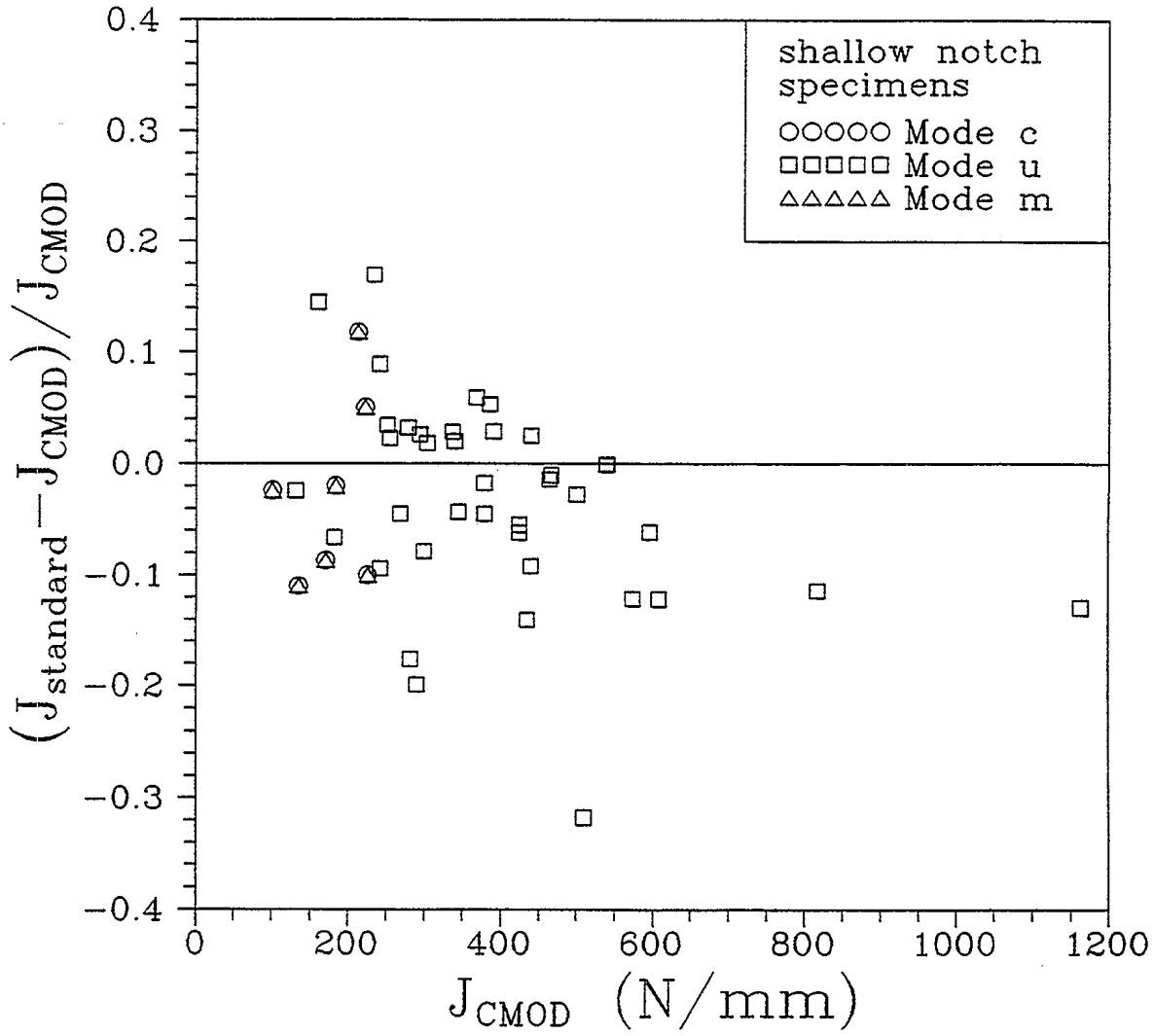

Figure 19 : $(J_{standard}-J_{CMOD})/J_{CMOD}$ versus J_{CMOD} for shallow notch specimens.

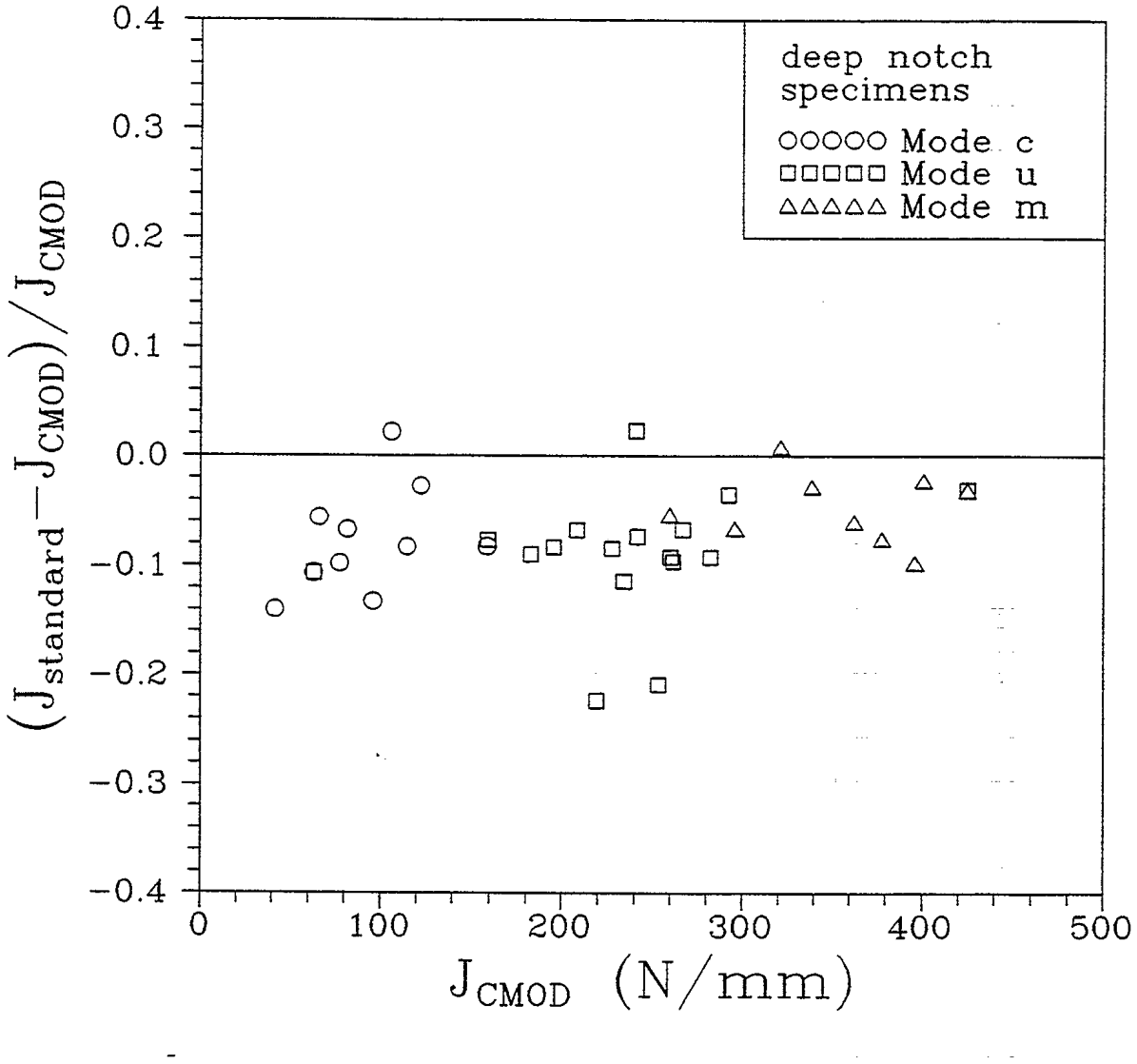

Figure 20: $(J_{standard}-J_{CMOD})/J_{CMOD}$ versus J_{CMOD} for deep notch specimens.